Journal of Catalysis 276 (2010) 197–200

Contents lists available at ScienceDirect

Journal of Catalysis

journal homepage: www.elsevier.com/locate/jcat

Priority Communication

Carbon monoxide-free hydrogen production via low-temperature steam reforming of ethanol over iron-promoted Rh catalyst

Luwei Chen [a,*], Catherine Kai Shin Choong [a,b], Ziyi Zhong [a], Lin Huang [a], Thiam Peng Ang [a], Liang Hong [b], Jianyi Lin [a]

[a] Institute of Chemical and Engineering Sciences, A*STAR (Agency for Science, Technology and Research), 1 Pesek Road, Jurong Island, Singapore 627833, Singapore
[b] Department of Chemical and Biomolecular Engineering, National University of Singapore, Singapore 117576, Singapore

ARTICLE INFO

Article history:
Received 9 June 2010
Revised 12 August 2010
Accepted 13 August 2010

Keywords:
Rh catalyst
Iron promotion
Hydrogen production
Steam reforming of ethanol

ABSTRACT

For the first time, a novel iron-promoted Rh catalyst is developed to produce CO-free H_2 through steam reforming of ethanol at low temperatures, between 623 and 673 K. The iron oxides in the vicinity of Rh sites reduce the CO adsorption on Rh sites and transfer the adsorbed CO from Rh to COO-formate species on Fe_xO_y for the subsequent water–gas shift reaction, resulting in a high H_2 yield, extremely low CO selectivity, and a long Rh life span.

1. Introduction

Hydrogen is used as a fuel for proton exchange membrane fuel cells (PEMFC) and phosphoric acid fuel cells (PAFC). It can be produced by on-site fuel reforming for stationary applications or onboard for automotive applications. A typical fuel processor is made up of different processing units such as fuel reformers and high-temperature and low-temperature water–gas shift (WGS) and CO cleanup reactors. WGS, as well as CO cleanup, is essential in fuel processors, since the electrodes can only tolerate about 1–2% CO for PAFC and less than 10 ppm for PEMFC [1,2]. PEMFC and PAFC are classified as low-temperature fuel cells, operating in low-temperature ranges, 353–393 K and 453–493 K, respectively. Therefore, it will be ideal if CO-free hydrogen can be produced at low temperatures. This can in turn lower the cost of the fuel processor by reducing the stacks of heat exchanger, WGS, or even CO cleanup processing units [1–3].

Renewable hydrogen produced via steam reforming of bioethanol (SRE) (Eq. (1)) has gained intense interest in recent years for the above applications [2–4]:

$$C_2H_5OH + 3H_2O \rightarrow 2CO_2 + 6H_2 \quad (1)$$

However, SRE is a complex process comprising many reactions that can be influenced by the properties of catalysts and the reaction conditions applied. Some of them are expressed in the following equations [5]:

$$C_2H_5OH \rightarrow CH_3CHO + H_2 \quad (2)$$

$$C_2H_5OH \rightarrow C_2H_4 + H_2O \quad (3)$$

$$CH_3CHO \rightarrow CH_4 + CO \quad (4)$$

$$CH_3CHO + H_2O \rightarrow 2CO + 3H_2 \quad (5)$$

$$CO + H_2O \leftrightarrow CO_2 + H_2 \quad (6)$$

$$CH_4 + H_2O \leftrightarrow CO + 3H_2 \quad (7)$$

Therefore, it is possible to alter the hydrogen yield and product selectivities by choosing proper catalysts and reaction conditions. Furthermore, catalyst deactivation, which is usually caused by the accumulation of carbonaceous deposits, is a serious problem during SRE, especially at low temperatures [6]. Several reactions responsible for coke formation have been proposed, as shown in the following equations:

$$2CO \leftrightarrow CO_2 + C \quad (8)$$

$$CH_4 \leftrightarrow 2H_2 + C \quad (9)$$

$$C_2H_4 \rightarrow \text{polymers} \rightarrow \text{coke} \quad (10)$$

Coking can be mitigated at high temperatures. Thus, SRE is usually operated in the temperature range 823–1073 K to avoid coking and

* Corresponding author. Fax: +65 6316 6182.
E-mail address: chen_luwei@ices.a-star.edu.sg (L. Chen).

0021-9517/$ - see front matter © 2010 Elsevier Inc. All rights reserved.
doi:10.1016/j.jcat.2010.08.018

to obtain high hydrogen yield [6]. However, CO formation would increase correspondingly with increasing temperature (>823 K) due to the thermodynamically favored reverse WGSR (Eq. (6)). Therefore, in order to reduce the CO concentration significantly, the reaction should proceed at relatively low temperatures. To do so, one should optimize the reaction condition by balancing SRE and WGSR and develop coking-resistant catalysts that can perform at low temperatures. Indeed, methane produced from ethanol decomposition (Eqs. (2) and (4)) cannot be converted to H_2 via steam reforming effectively (Eq. (7)) at low temperatures. Therefore, the yield of H_2 is lower than that at high reforming temperatures (above 773 K). However, the energy efficiency of low-temperature SRE could remain high if methane and carbon oxides could be separated from hydrogen and sent to the tail gas combustion chamber to generate heat for the reformer [2,7].

Some supported noble metal catalysts have been reported for the low-temperature SRE [3,7–11]. Basagiannis et al. reported that 0.5% Pt/Al_2O_3 was the best among catalysts of Rh, Ru, Pt, and Pd supported on Al_2O_3. However, the selectivity to CO was as high as 30% at 623 K [7]. In another study, a H_2 yield of 1.99 mol H_2/mol EtOH with a CO selectivity of 1.5% was achieved at 673 K over a 1.5% $Pt/Ce_{0.8}Zr_{0.2}O_2$ catalyst [3]. Roh et al. reported a H_2 yield of 4.3 mol H_2/mol EtOH with CO selectivity of 10% over a 2% $Rh/Ce_{0.8}Zr_{0.2}O_2$ catalyst at 723 K [8]. A bimetallic Rh–Pd/CeO_2 catalyst was reported to exhibit good performance at 777 K. However, the addition of Pd did not decrease the selectivity of CO, which remained as high as 42.8% at 580 K [9]. In one of our recent reports, 1% Rh supported on hydrothermally synthesized ZrO_2 could produce high H_2 yield in the temperature range 573–673 K; however, the selectivity to CO is about 30%, and catalyst deactivation was observed at temperatures below 673 K due to the accumulation of CO, carbonate, and CH_x on the catalyst surface [10]. Despite the high activity shown by noble metal catalysts for the SRE at low temperatures, CO is inevitable in the final products.

In this communication, we report a novel multifunctional iron-oxide-promoted catalyst, Rh–Fe/Ca–Al_2O_3, for the low-temperature SRE process. Significant increase in H_2 yield and extremely low CO selectivity can be achieved in the presence of iron promoter. A plausible reaction mechanism and the role of iron oxides are also discussed.

2. Experimental

The Rh–Fe/Ca–Al_2O_3 catalyst was prepared by a sequential incipient wetness impregnation method, following the steps given below: (1) Ca-modified alumina, denoted as Ca–Al_2O_3, was prepared by the calcination of a paste of γ-Al_2O_3 (Merck, 103 m^2/g) impregnated with $Ca(NO_3)_2{\cdot}4H_2O$ (Riedel–deHaën) solution. (2) The obtained Ca–Al_2O_3 powder was impregnated with an appropriate amount of $Fe(NO_3)_3$ solution to get a precursor with Fe loading of 10 wt.%. The precursor was dried at 393 K for 10 h and heated to 723 K in air and then held for 5 h. (3) By impregnation with a $RhCl_3$ solution (Alfa Aesar), 1 wt.% of Rh was introduced into the powder obtained in step (2). The obtained catalyst was dried and calcined in the same manner as in step (2) and is denoted as Rh–Fe/Ca–Al_2O_3. For comparison, an Fe-free 1 wt.% Rh catalyst, denoted as Rh/Ca–Al_2O_3, was also prepared, following steps (1) and (3).

The activity measurements were carried out by using a microquartz tube reactor equipped with an online Varian CP-3800 gas chromatograph (GC). Prior to the reaction, catalysts were reduced in pure H_2 with a flow of 50 ml/min at 473 K for 0.5 h. During the reaction, a liquid mixture of EtOH/H_2O = 1:3 (v:v) was fed into a vaporizer (443 K) at 0.005 ml/min with Ar (40 ml/min) as carrier gas. The gas hourly space velocity (GHSV) was 34,000 h^{-1}, and the weight hourly space velocity (WHSV) was 0.54 $g_{EtOH}g_{Cat}$/h. The GC for online outlet gas analysis had two channels with two thermal conductivity detectors. One channel with carrier gas Ar was used for analyzing H_2, CH_4, and CO using a 5-Å molecular sieve column, and the other channel with carrier gas He was equipped with a Hayesep Q column for the separation of C_2H_5OH, CH_3CHO, CO_2, C_2H_4, C_2H_6, acetone, and H_2O. Conversion of ethanol (X_{EtOH}) and selectivity to carbon-containing species (S_{Ci}) were calculated as follows:

$$X_{EtOH} = \left(1 - \frac{2 \times \mathrm{mol}_{EtOH_{out}}}{\sum_i^n \mathrm{molC}_i + 2 \times \mathrm{mol}_{EtOH_{out}}}\right) \times 100\% \quad (11)$$

$$S_{C_i} = \frac{\mathrm{molC}_i}{\sum_i^n \mathrm{molC}_i} \times 100\%, \quad (12)$$

where C_i represents a C-containing product. The selectivity S_{ci} was calculated based on detected carbon only, assuming that no coke was formed during the reaction. H_2 yield (Y_{H2}) was evaluated in terms of the number of moles of H_2 produced per mole of fed ethanol.

Dispersion of Rh was measured by pulse H_2 (99.999%) chemisorption using a thermal conductivity detector (Thermo, TPDRO 1100). Catalysts were reduced at 473 K for 0.5 h (the same as for catalytic activity measurement) and then purged with Ar at 673 K for 1 h and cooled to 298 K. At 298 K, pulses of H_2 were introduced. Moles of active Rh were obtained assuming that each Rh atom chemisorbs one hydrogen atom.

In situ diffuse reflectance infrared Fourier transform spectroscopy (DRIFTS) study of CO adsorption was carried out in a Bio-Rad FT-IR 3000 MX with a mercury-cadmium-telluride (MCT) detector. A powder sample was put into a reaction cell (Harricks HV-DR2) and reduced under the same conditions as for the activity test. A flow of 1% CO/He was introduced at room temperature after the sample had been purged by He for 0.5 h after the reduction. Spectra with a resolution of 4 cm^{-1} were taken after CO had been adsorbed for 0.1 h.

Powder X-ray diffraction (XRD) patterns were collected with a Bruker D8 X-ray diffraction system equipped with Cu Kα radiation (λ = 0.154 nm). The profiles were collected at a step width of 0.02° in the (2θ) range from 20° to 90°. Transmission electron microscopy (TEM) was done on a FEI Tecnai G^2 microscope. X-ray photoelectron spectroscopy (XPS) was performed on a VG ESCALAB 250 spectrometer using an Mg Kα radiation source. The XPS data were processed with respect to the adventitious carbon C1*s* peak at 284.5 eV. The TEM, XRD, and XPS results are given in the Supplementary information.

3. Results and discussion

The TEM image (Fig. S1b in the Supplementary information) shows the coexistence of well-crystallized Rh and Fe_2O_3 nanoparticles on the reduced Rh–Fe/Ca–Al_2O_3 catalyst. The XRD (Fig. S2) pattern consistently confirms the formation of the α-Fe_2O_3 phase. The XPS spectrum of as-calcined Rh–Fe/Ca–Al_2O_3 (Fig. S3a) shows an Fe2$p_{3/2}$ peak centered at 711.2 eV, corresponding to Fe(III). After reduction at 473 K for 0.5 h, the Fe2$p_{3/2}$ peak broadens (Fig. S3b) because of the extra contribution from Fe(II), which indicates the formation of Fe_3O_4 or probably coordinatively unsaturated iron sites on the reduced catalyst surface [12,13]. Ca has been introduced into the Al_2O_3 support to neutralize the acidity of Al_2O_3, since it will result in the dehydration of ethanol (Eq. (3)) and subsequently the polymerization of C_2H_4 (Eq. (10)) on the catalyst [5].

The performance of the Rh–Fe/Ca–Al_2O_3 and Rh/Ca–Al_2O_3 catalysts is compared in terms of Y_{H2} (yield of H_2), X_{EtOH} (ethanol conversion), S_x (selectivities to products *x*), TOF_{EtOH}, and TOF_{H2}, as listed in Table 1. At 573 K, for the Rh/Ca–Al_2O_3 catalyst, the main

products are CO, CH_4, CO_2, C_2H_4, and CH_3CHO, with an X_{EtOH} of 63.5%; the selectivity is 50.2% to CO and 40.0% to CH_4, respectively. S_{CO} is higher than S_{CH4}, indicating a low reaction rate for the WGSR (Eq. (6)) and a high rate for methane decomposition (Eq. (9)) on the Rh/Ca–Al_2O_3 catalyst. The results are similar to those observed for an Rh–Pd/CeO_2 catalyst reported by Scott et al. [9] and an Rh/Al_2O_3 catalyst reported by Cavallaro [11]. For the Rh–Fe/Ca–Al_2O_3 catalyst operated at the same temperature, X_{EtOH} increases greatly from 63.5% (Fe-free) to 99.3% with an Y_{H2} of 3.5 mol; S_{CO} decreases significantly from 50.2% (Fe-free) to 12.3%, accompanied by an increase in S_{CO2} from 2.5% to 43.0%, while S_{CH4} remains almost unchanged. At 623 K, X_{EtOH} reaches 93.4% over Rh/Ca–Al_2O_3 without detection of acetaldehyde. In addition, S_{CO} and S_{CH4} are almost unchanged compared to those detected for the same catalyst at a lower temperature, 573 K, indicating that the reaction pathway remained the same. On the other hand, Rh–Fe/Ca–Al_2O_3 produces extremely low S_{CO} at 623 K with almost no detection of CO, while S_{CO2} reaches 60.3% and Y_{H2} as high as 4.1 mol is measured.

In short, Y_{H2} has increased significantly with the decrease in CO on the iron-promoted Rh catalyst. We argue that CO, which was derived from CH_3CHO decarbonation (Eq. (4)), may be converted by three reactions: the WGS reaction (Eq. (6)), the methanation reaction (Eq. (7), reversed methane steam reforming), and the Boudouard reaction (Eq. (8)). The last possibility can basically be excluded, as it only occurs on metallic Fe particles [14]. In our XPS and XRD experiments (Figs. S2 and S3), we did not detect any metallic Fe phase in the catalysts. In comparison with the Fe-free catalyst, both S_{CO2} and Y_{H2} increase significantly on the Rh–Fe/Ca–Al_2O_3 catalyst with the decrease in S_{CO}, while S_{CH4} remains almost unchanged. Since iron oxide is a well-known WGSR catalyst, it is reasonable to propose that the addition of iron oxides remarkably promoted the WGSR (Eq. (6)), resulting in the improved Y_{H2} and reduced CO production at low temperatures. The tests of WGSR on the Rh/Ca–Al_2O_3 and Rh–Fe/Ca–Al_2O_3 catalysts prove this hypothesis (see Fig. S4 in the Supplementary information). The conversion of CO is only 6% over the Rh/Ca–Al_2O_3 catalyst at 573 K, while it increases dramatically to 88% over the Rh–Fe/Ca–Al_2O_3 catalyst. A similar observation on the promotion effect of iron for the WGSR during SRE has been reported in a bimetallic 10% Co–1% Fe/ZnO catalyst, which showed slightly higher activity for WGSR at low temperature than 10% Co/ZnO and 10% Co–1% Ni/ZnO catalysts [15].

At 673 K, over the Rh/Ca–Al_2O_3 catalyst, Y_{H2} increases to 4.7 mol, and S_{CO} and S_{CH4} decreases to 15.7% and 28.8%, respectively, all of which may result from the enhancement of reaction rate at higher temperatures. Over the Rh–Fe/Ca–Al_2O_3 catalyst, Y_{H2} is 4.3 mol, which is surprisingly slightly lower than that for Rh/Ca–Al_2O_3 (4.7 mol), and there is still no detection of CO. The Y_{H2} might have been higher than that for Rh/Ca–Al_2O_3 if CO were completely converted into CO_2 and H_2 by the WGSR (Eq. (6)). Hence, a lower Y_{H2} here implies that, besides the WGSR, there exists another reaction pathway. CO may be converted to CH_4 via the methanation reaction (Eq. (7)), which is thermodynamically favorable at relatively low temperatures. Indeed, we observe 7.4% increase in S_{CH4} and a slight decrease in Y_{H2} on the Fe-promoted catalyst.

The data in Table 1 have demonstrated that CO-free H_2 gas can be produced directly from the SRE on the Rh–Fe/Ca–Al_2O_3 catalyst in the temperature range 623–673 K. More importantly, the stability study presented in Fig. 1 indicates that the addition of iron oxide to the Rh/Ca–Al_2O_3 catalyst can greatly enhance its life span. As shown in Fig. 1, the Rh–Fe/Ca–Al_2O_3 catalyst is stable for the SRE

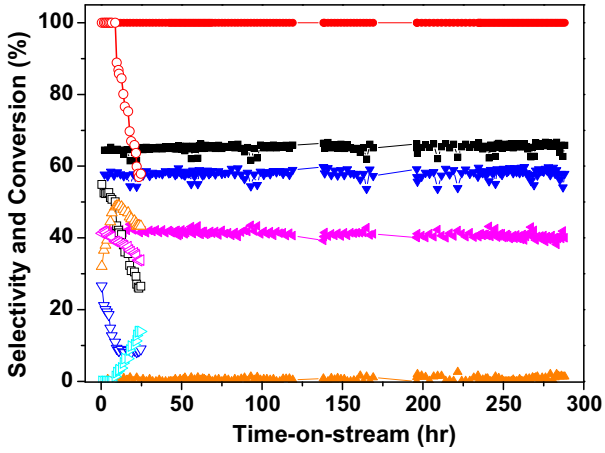

Fig. 1. Conversion of ethanol and selectivity of products as function of time on stream over Rh–Fe/Ca–Al_2O_3 (solid) and Rh/Ca–Al_2O_3 (open) at 623 K and 1 atm (●X_{EtOH}, ■S_{H2}, ▲S_{CO}, ▼S_{CO2}, ◄S_{CH4}, and S_{CH3CHO}).

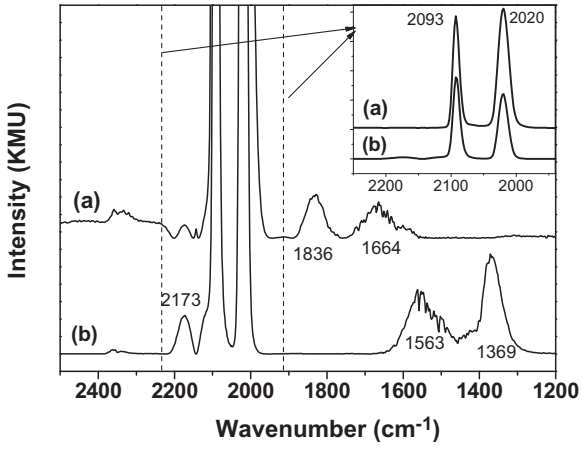

Fig. 2. DRIFT spectra recorded under 1% CO/He at 298 K after H_2 treatment of Rh/Ca–Al_2O_3 (a) and Rh–Fe/Ca–Al_2O_3 (b) at 298 K.

Table 1
Activity of catalysts at 573, 623, and 673 K.

T (K)	Catalysts	Y_{H2} (H_2/EtOH (mol/mol))	X_{EtOH} (%)	S_{CO2} (%)	S_{CO} (%)	S_{CH4} (%)	S_{C2H4} (%)	S_{CH3CHO} (%)	TOF_{ETOH} (s^{-1})[a]	TOF_{H2} (s^{-1})[b]
573	Rh/Ca–Al_2O_3	1.8	63.5	2.5	50.2	40.0	0.19	7.1	0.037	0.066
	Rh–Fe/Ca–Al_2O_3	3.5	99.3	43.0	12.3	44.7	0.0	0.0	0.122	0.427
623	Rh/Ca–Al_2O_3	3.6	93.4	16.7	47.0	36.4	0.0	0.0	0.054	0.194
	Rh–Fe/Ca–Al_2O_3	4.1	100.0	60.3	0.0	39.7	0.0	0.0	0.123	0.503
673	Rh/Ca–Al_2O_3	4.7	100.0	55.5	15.7	28.8	0.0	0.0	0.058	0.271
	Rh–Fe/Ca–Al_2O_3	4.3	100.0	63.8	0.0	36.2	0.0	0.0	0.123	0.528

[a] Molecules of EtOH converted per Rh surface atom per second.
[b] Molecules of H_2 produced per Rh surface atom per second.

reaction at 623 K for 288 h. In contrast, deactivation is observed for the Rh/Ca–Al_2O_3 catalyst after a 7.5-h reaction, accompanied by obvious increments in the CH_3CHO and CO selectivity. It has been proposed in several papers that the reaction/adsorption of ethanol over Rh catalysts first undergoes dehydrogenation to acetaldehyde and hydrogen (Eq. (2)). Acetaldehyde intermediates quickly decarbonylate into CO and CH_4 due to the active C–C rupture property of Rh (Eq. (4)). Finally, CH_4 may convert to CO and H_2 by steam reforming (Eq. (7)) or decompose to C and H_2 by cracking (Eq. (9)), while CO may convert into CO_2 and H_2 by the WGSR (Eq. (6)) [7–10,16]. An increase in CH_3CHO production indicates that the surface Rh atoms have gradually lost the ability to break the C–C bond of CH_3CHO, which may be attributed to the poisoning effect of strong CO–Rh bonding and hence the blockage of $Rh\mu^2[\eta^2(C, O)]$ active sites for C–C bond activation and rupture [17,18].

In situ DRIFTS studies of CO adsorption support the above hypothesis. As shown in Fig. 2a, two strong bands at 2093 and 2020 cm^{-1}, which are exactly the same as those reported by Erdöhelyi and Solymosi on a 0.3% Rh/Al_2O_3 catalyst [19], are observed for the Rh/Ca–Al_2O_3 catalyst. They are assigned to asymmetric and symmetric stretch of gem-dicarbonyls on Rh ions, respectively. The strength of the Rh–CO bond energy in gem-dicarbonyl is ~145 kJ/mol, even greater than the 121 kJ/mol of Rh–Rh bonds in metallic Rh [20]. The high concentration of gem-dicarbonyl CO that may remain on the Rh surface at temperatures < 503 K will poison the Rh active sites for ethanol adsorption and further acetaldehyde decomposition. At higher temperatures, CO may undergo the Boudouard reaction (Eq. (8)), thus depositing carbon and poisoning the catalyst. Two smaller bands at 1836 and 1664 cm^{-1} can be attributed to bridged Rh_2–CO and tilted CO [21]. The other smaller bands at 2141 and 2172 cm^{-1} can be assigned to $Rh^{2+}(CO)_2$ [21].

For the Rh–Fe/Ca–Al_2O_3 catalyst, the concentration of gem-dicarbonyl CO is mitigated (see the inset of Fig. 2) so that the CO poisoning effect can be reduced. In addition, it is noted that the bridged and tilted CO adsorption bands disappear in Fig. 2b, while two new bands at 1554 and 1372 cm^{-1}, which can be attributed to ν_a(OCO) and ν_s(OCO) of formate species on iron oxide surface, are evidently observed [22]. These peak changes suggest that adsorbed CO species on Rh sites can be converted to COO^- species in the presence of iron oxide, which is an excellent catalyst for the WGSR and is now located adjacent to Rh, as shown by the TEM image (Fig. S1 in the Supplementary information).

The above IR spectroscopic changes caused by the addition of iron oxides clearly indicate that in the presence of iron oxide, adsorbed CO species on Rh sites can be converted to COO^- species or gaseous CO_2 (so that the overall number of adsorbed CO species is reduced). We can thus propose a reaction mechanism for the SRE process over Rh–Fe/Ca–Al_2O_3. Ethanol adsorption and activation mainly occur at Rh active sites. Hence, CO that are derived from CH_3CHO reforming (Eq. (5)) and decarbonation (Eq. (4)) are bonded to Rh sites. As CO–Rh bonding is very strong, without the presence of Fe oxides, the subsequent WGSR proceeds slowly at low temperatures, even though thermodynamically CO should be converted to CO_2 in the presence of water. The strong CO–Rh bonding results in undesired high CO selectivity over iron-free Rh catalysts and the deactivation of the Rh catalyst. In the presence of Fe_xO_y, CO adsorbed onto Rh particles can migrate from Rh to the nearby Fe_xO_y. As can be seen from the XPS results in the Supplementary information, Fe_xO_y are easily generated by H_2 reduction at 200 °C. Therefore, coordinatively unsaturated ferrous (CUF) can form along the interface between Rh and Fe_xO_y. The WGSR can proceed following the reaction scheme:

$$H_2O + * \rightarrow 2OH_a \rightarrow 2O_a + H_2 \quad (13)$$

$$CO + O_a \rightarrow CO_{2a} \rightarrow CO_2 + * \quad (14)$$

where O_a represents a lattice oxide ion, CO_{2a} and OH_a are adsorbed species, and * denotes a surface vacancy, which may be a CUF site. The addition of iron oxides enables our novel catalyst to play bifunctional roles at the molecular level for SRE and the WGSR. This would enhance the ethanol conversion, eliminate the CO production, which is an undesired product and an Rh catalyst poison, and improve the catalyst stability. This mechanism is very similar to the interface-confined ferrous centers for catalytic CO oxidation that was very recently reported by Fu et al. [13]. In their paper, CO bonding energy at coordinatively unsaturated ferrous (CUF) on the FeO/Pt interface was found to be smaller than that on FeO-free Pt surface. Therefore, adsorbed CO on FeO/Pt is unstable and can quickly react by O_2 exposure. O_2 can be preferentially adsorbed and activated at CUF. The adsorbed O at the CUF sites can react with CO adsorbed on neighboring Pt atoms, and CO oxidation can thus proceed on FeO/Pt. On pure Pt surfaces, the active Pt sites are blocked by strongly adsorbed CO, and no oxidation can take place at modest temperatures.

4. Conclusions

We have demonstrated that CO-free H_2 can be produced through low-temperature (623–673 K) steam reforming of bioethanol on an Rh–Fe/Ca–Al_2O_3 catalyst. The role of iron oxide is to enhance the WGSR, which can efficiently convert CO byproduct to CO_2 and H_2. Furthermore, the presence of Fe_xO_y is able to improve the durability of the catalyst by the mitigation of CO poisoning of Rh.

Acknowledgments

The authors thank the Science and Engineering Research Council of A*STAR (Agency for Science Technology and Research), Singapore, for financial support, Dr. Yi-Fan Han for valuable discussion on the manuscript preparation, Zhan Wang for the XPS measurement, and Jaclyn Teo for the WGSR test.

Appendix A. Supplementary material

Supplementary data associated with this article can be found, in the online version, at doi:10.1016/j.jcat.2010.08.018.

References

[1] C. Song, Catal. Today 77 (2002) 17.
[2] B.J. Bowers, J.L. Zhao, M. Riffo, R. Khan, D. Dattatraya, N. Dushman, J. Beziat, F. Boudjemaa, Int. J. Hydrogen Energy 32 (2007) 1437.
[3] Y. Chen, Z. Shao, N. Xu, Energy Fuels 22 (2008) 1873.
[4] U. Eberle, M. Felderhoff, F. Schüth, Angew. Chem. Int. Ed. 48 (2009) 6608.
[5] A. Haryanto, S. Fernando, N. Murali, S. Adhikari, Energy Fuels 19 (2005) 2098.
[6] A.L. da Silva, C.deF. Malfatti, I.L. Müller, Int. J. Hydrogen Energy 34 (2009) 4321.
[7] A.C. Basagiannis, P. Panagiotopoulou, X.E. Verykios, Top. Catal. 51 (2008) 2.
[8] H. Roh, Y. Wang, D.L. King, A. Platon, Y. Chin, Catal. Lett. 108 (2006) 15.
[9] M. Scott, M. Geoffroy, W. Chiu, M.A. Blackford, H. Idriss, Top. Catal. 51 (2008) 13.
[10] Z.Y. Zhong, H. Ang, C. Choong, L. Chen, L. Huang, J. Lin, Phys. Chem. Chem. Phys. 11 (2009) 872.
[11] S. Cavallaro, Energy Fuels 14 (2000) 1195.
[12] C.S. Kuivila, J.B. Butt, P.C. Stair, Appl. Surf. Sci. 32 (1988) 99.
[13] Q. Fu, W. Li, Y. Yao, H. Liu, H. Su, D. Ma, X. Gu, L. Chen, Z. Wang, H. Zhang, Bing Wang, X. Bao, Science 328 (2010) 1141.
[14] Z.Y. Zhong, J. Highfield, M. Lin, J. Teo, Y.F. Han, Langmuir 24 (2008) 8576.
[15] A. Casanovas, M. Roig, C. Leitenburg, A. Trovarelli, J. Llorca, Int. J. Hydrogen Energy 35 (2010) 7690.
[16] J. Rasko, A. Hancz, A. Erdohelyi, Appl. Catal. A 269 (2004) 13.
[17] N.F. Brown, A. Barteau, J. Am. Chem. Soc. 114 (1992) 4258.
[18] S.M. Gates, J.N. Russell Jr., J.T. Yates Jr., Surf. Sci. 171 (1986) 111.
[19] A. Erdöhelyi, F. Solymosi, J. Catal. 84 (1983) 446.
[20] R. Krishnamurthy, S.S.C. Chuang, Thermochim. Acta 262 (1995) 215.
[21] S.S.C. Chuang, R.W. Stevens Jr., R. Khatri, Top. Catal. 32 (2005) 225.
[22] V. Galvita, L.K. Rihko-Struckmann, K. Sundmacher, J. Mol. Catal. A 283 (2008) 43.